Suppression of Dynamically Induced Stochastic Magnetic Behaviour through Materials Engineering

Supplementary Material

IFD and DFD histograms for all devices measured:

Figures S1 – S4 below present IFD and DFD histograms for each of the viable devices measured in this study. Devices are grouped by defect geometry, with data for the undoped $Ni_{80}Fe_{20}$ and 5% Tb-doped nanowires shown in adjacent panels to aid comparison.

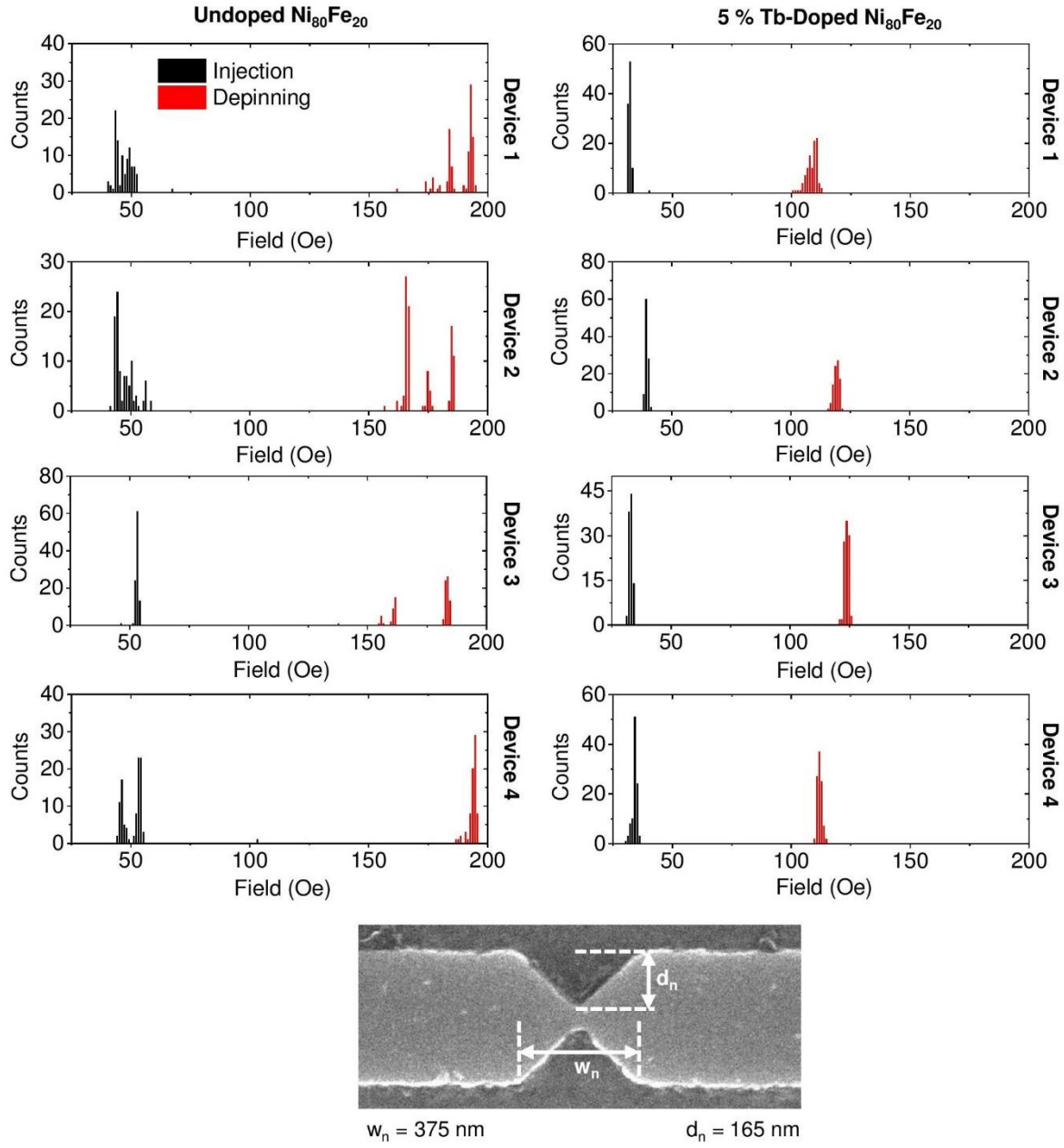

Figure S1: IFD and DFD histograms measured from nanowires containing notch-shaped artificial defect sites with w_n = 375 nm and d_n = 165 nm.

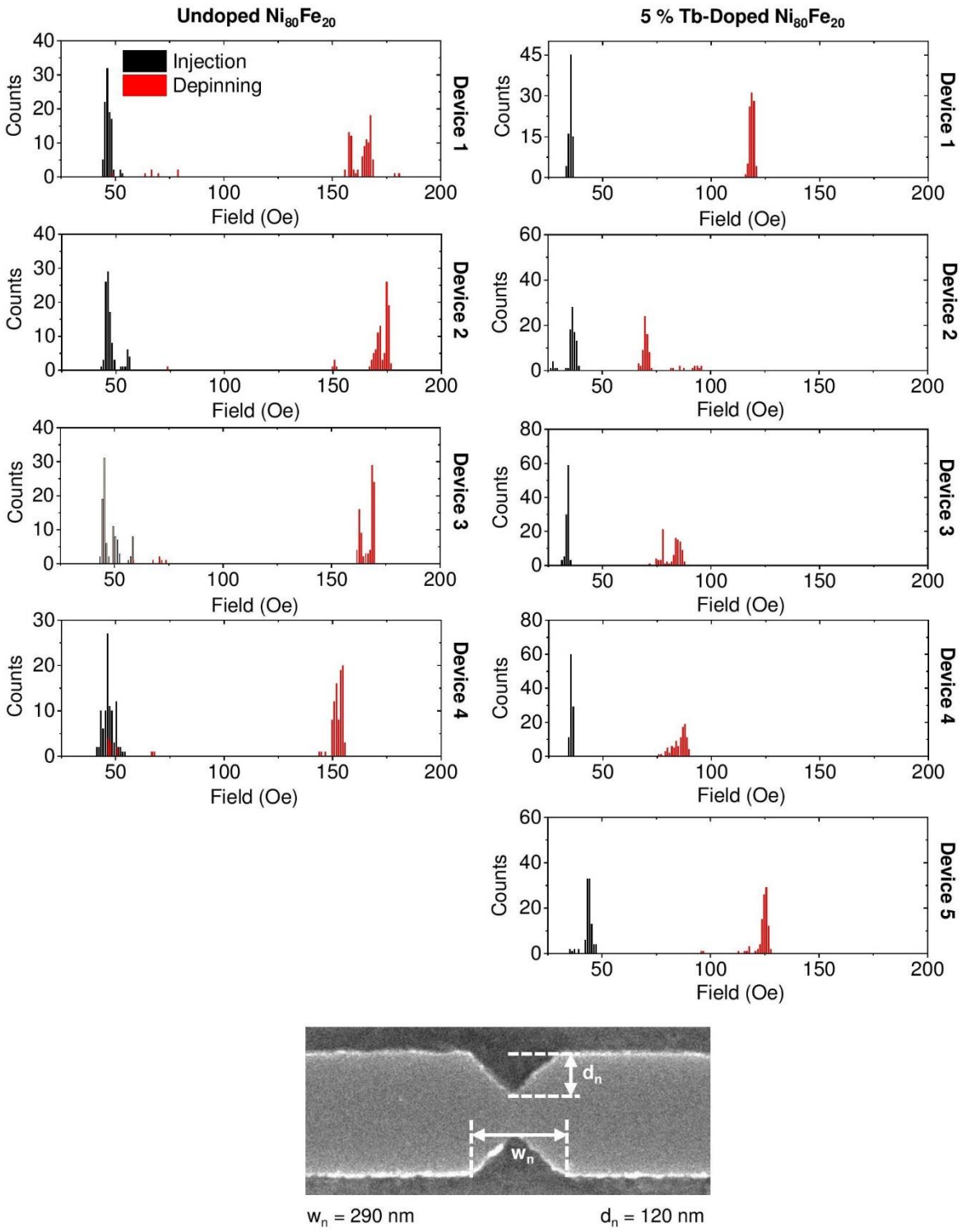

Figure S2: IFD and DFD histograms measured from nanowires containing notch-shaped artificial defect sites with w_n = 290 nm and d_n = 120 nm.

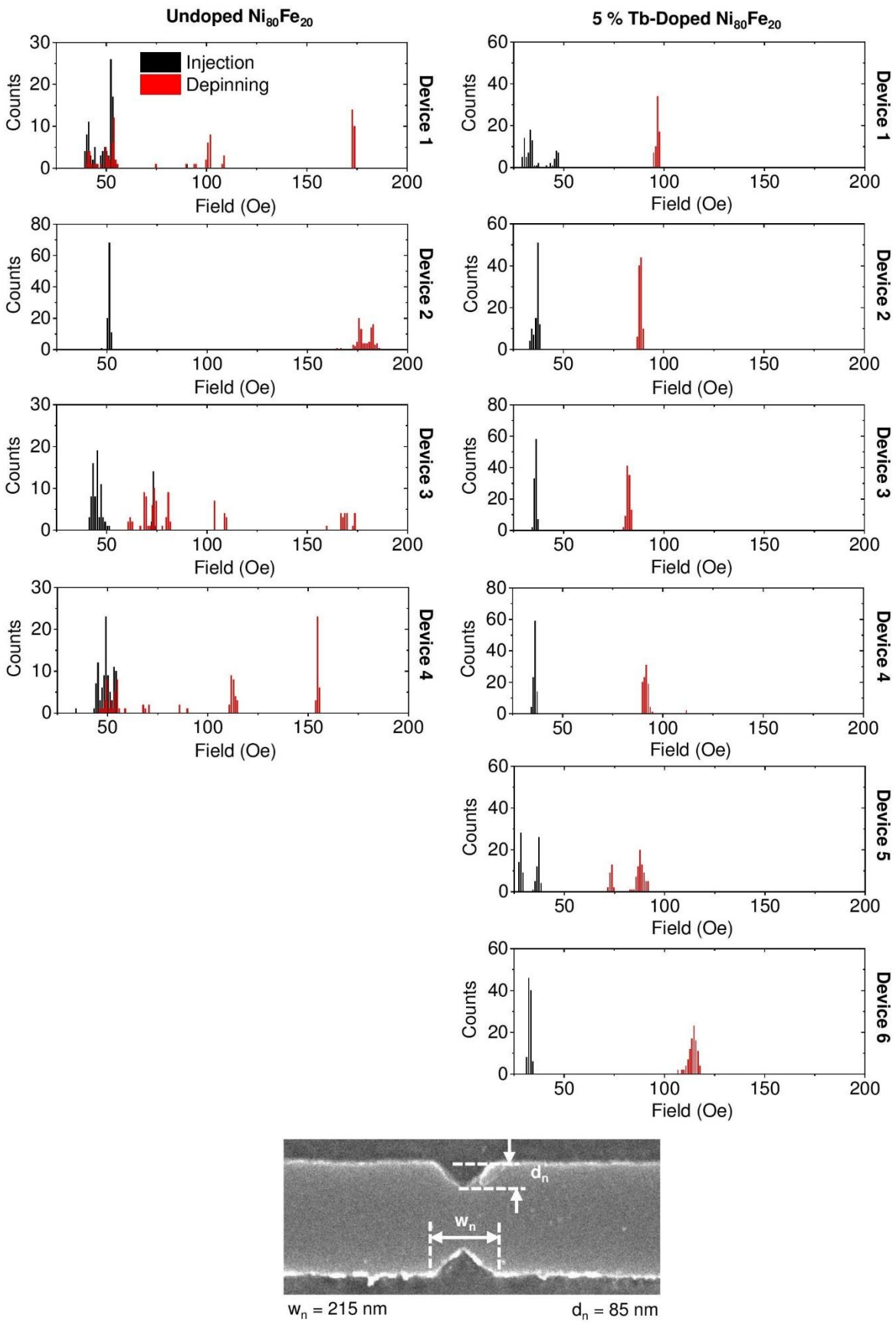

Figure S3: IFD and DFD histograms measured from nanowires containing notch-shaped artificial defect sites with w_n = 215 nm and d_n = 85 nm.

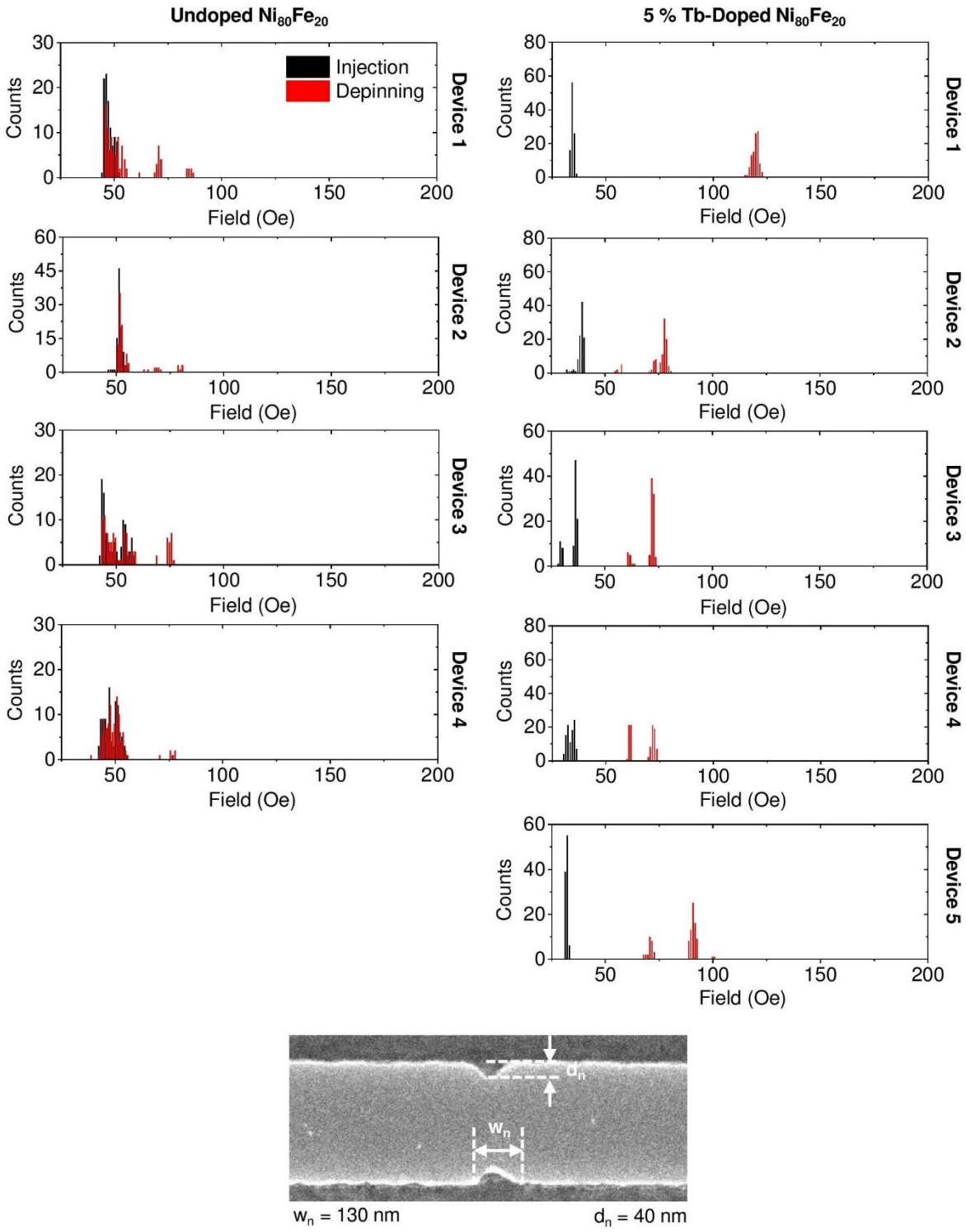

Figure S4: IFD and DFD histograms measured from nanowires containing notch-shaped artificial defect sites with w_n = 130 nm and d_n = 40 nm.

Numerical parameters for all devices measured:

d_n (nm)	Device number	H_{inject} (Oe)	σ_{inject} (Oe)	$\sigma_{inject}/H_{inject}$	H_{depin} (Oe)	σ_{depin} (Oe)	σ_{depin}/H_{depin}
165	1	47	3.9	0.083	188	6.3	0.034
	2	47	4.2	0.087	173	8.7	0.050
	3	53	0.9	0.017	175	11.8	0.067
	4	51	6.5	0.126	196	4.1	0.021
120	1	47	1.5	0.032	157	25.2	0.161
	2	48	3.2	0.067	171	11.2	0.066
	3	48	4.3	0.089	161	23.6	0.147
	4	47	2.6	0.056	141	31.9	0.226
85	1	49	5.2	0.108	94	51.3	0.545
	2	51	0.6	0.013	179	3.8	0.022
	3	50	11.2	0.222	97	39.1	0.401
	4	49	3.4	0.070	102	43.1	0.422
40	1	47	3.2	0.067	55	11.6	0.210
	2	52	1.3	0.026	55	8.1	0.146
	3	49	5.1	0.103	54	11.1	0.203
	4	48	3.4	0.069	50	7.1	0.142

Table S1: Numerical IFD and DFD parameters for $Ni_{80}Fe_{20}$ nanowires.

w_n (nm)	Device number	H_{inject} (Oe)	σ_{inject} (Oe)	$\sigma_{inject}/H_{inject}$	H_{depin} (Oe)	σ_{depin} (Oe)	σ_{depin}/H_{depin}
165	1	32	1.0	0.031	108	2.3	0.022
	2	40	0.59	0.015	119	1.2	0.0097
	3	33	0.73	0.022	123	0.9	0.0076
	4	34	1.06	0.031	112	1.0	0.0090
120	1	35	0.7	0.020	118	1.0	0.008
	2	36	2.7	0.074	73	8.0	0.110
	3	34	0.7	0.022	82	4.0	0.049
	4	36	0.6	0.016	85	3.1	0.037
	5	44	2.1	0.048	124	4.7	0.038
85	1	36	6.2	0.171	96	0.8	0.009
	2	37	1.2	0.034	88	0.7	0.007
	3	36	0.5	0.015	82	0.9	0.010
	4	36	0.6	0.018	92	3.1	0.034
	5	33	4.4	0.136	84	6.7	0.080
	6	33	0.7	0.021	114	2.2	0.019
40	1	35	0.6	0.018	119	1.5	0.013
	2	39	1.6	0.041	75	5.8	0.077
	3	35	2.8	0.081	70	3.8	0.053
	4	34	1.7	0.052	67	5.5	0.082
	5	32	0.6	0.018	85	9.3	0.108

Table S2: Numerical IFD and DFD parameters for 5 % Tb-doped $Ni_{80}Fe_{20}$ nanowires.

Plot of σ_{depin}/H_{depin} as a function of notch depth:

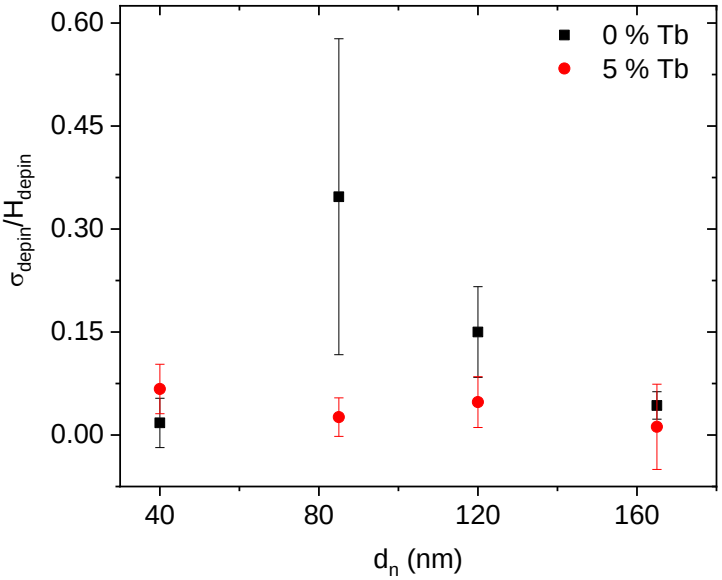

Figure S5: Plot of σ_{depin}/H_{depin} as a function of notch depth, d_n for the undoped $Ni_{80}Fe_{20}$ (black circles) and 5 % Tb-doped (red circles) nanowires. Error bars in all three figures represent standard deviation rather than standard error in order to give the reader a clear indication of the spread of values across the devices measured.

Study of correlation between splitting of IFDs and DFDs in Tb-doped Nanowires.

Visual inspection was used to identify whether the IFD and DFD were split into two or more modes for each of the nanowires studied, producing the results shown in Table S3. These data were then used to form the contingency table presented in Table S4. For a null hypothesis that splitting of the DFD and IFD are uncorrelated we obtain a Pearson's $\chi^2 = 5.09$ and p-value = 0.024. We thus reject the null hypothesis at $P < 0.05$.

Notch Size (nm)	Device Number	IFD Split?	DFD Split?
165	1	No	No
	2	No	No
	3	No	No
	4	No	No
120	1	No	No
	2	Yes	Yes
	3	No	Yes
	4	No	No
	5	Yes	Yes
85	1	Yes	No
	2	No	No
	3	No	No
	4	No	Yes
	5	Yes	Yes
	6	No	No
40	1	No	No
	2	No	Yes
	3	Yes	Yes
	4	Yes	Yes
	5	No	Yes

Table S3: Data indicating whether the IFD and DFD were determined to be split into two or more modes for each of the Tb-doped viable nanowires measured in this study.

	DFD not split	DFD split	Total
IFD not split	10	4	14
IFD split	1	5	6
Total	11	9	20

Table S4: Contingency table examining the correlation between IFD and DFD splitting in the Tb-doped nanowires. The table summarises the number of devices in which the DFD/IFD was split/ not split as determined by visual inspection of the histograms.

Simulations of pinning at d_n = 40 nm defect sites

To perform simulations of DW pinning at defect sites with realistic geometries, the d_n = 40 nm defect geometry shown in Figure 4(d) was traced from an SEM image and introduced into a simulation of a 4000 x 4000 x 20 nm^3 nanowire. DWs were relaxed at the left-hand side of the simulation and propagated to the defect site at H = 35 Oe, the average IFD value for the 5 % Tb-doped devices. Once the DWs had pinned at the defect site, the applied field was quasi-statically ramped in 5 Oe steps to determine the DWs depinning field. Simulations were performed for six distinct initial DW structures: TDW UP, TDW DOWN, CW VDW (vortex core up), CW VDW (vortex core down), ACW VDW (vortex core up) and ACW VDW (vortex core down).

Figure S6(a) illustrates plots of M_x/M_s vs field for each of the pinned DW configurations. Three distinct DW depinning fields were observed: H = 60 Oe (ACW VDW with core up/down), H = 75 Oe (CW VDW with core down) and 85 Oe (TDW UP, TDW DOWN, CW VDW with core up). Figures S6(b)-(g) illustrate the magnetisation configurations observed during the switching of the nanowires for each initial DW configuration.

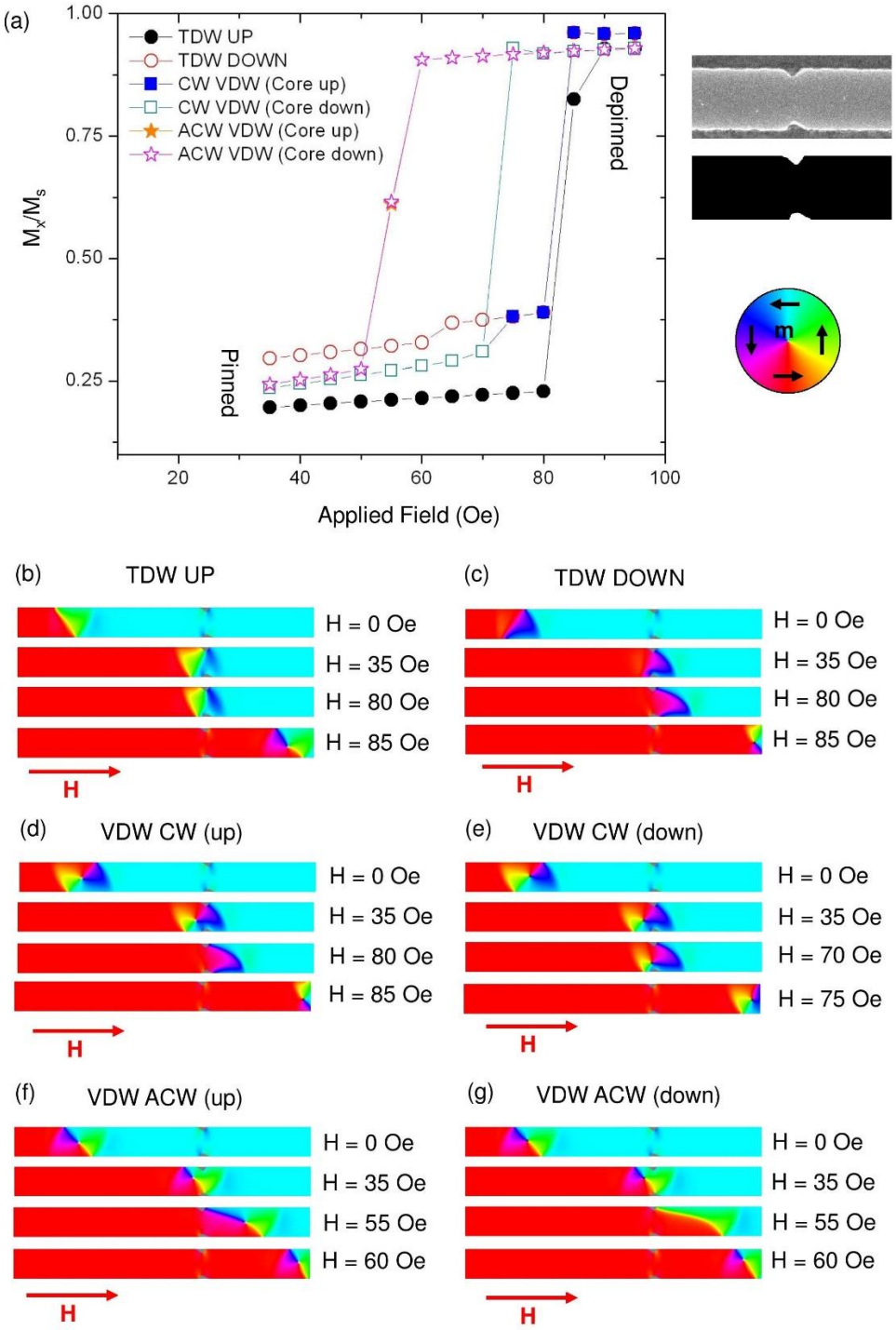

Figure S6: (a) Simulated plots of M_x/M_s vs applied field illustrating the depinning of DWs from a d_n = 40 nm defect site. Data is shown for six distinct DW configurations, corresponding to each of the DW magnetisation structures that were stable in the simulated nanowires. Data points for ACW VDW (Core up) are obscured by the data for ACW VDW (Core down), which are almost exactly coincident. The figures on the right-hand side of the plot present an SEM of simulated defect (upper image) and the image used to reproduce the defect in the simulation (lower image). (b)-(g) Magnetisation configurations illustrating the pinning and depinning processes of the DWs. Four images are shown for each initial DW configuration: the DW prior to propagation to the defect, the DW pinned at the defect site, the DW at an applied field value just below the depinning field and the DW after depinning